AFRL-ML-WP-TP-2006-445

MAXWELL GARNETT MODEL FOR DIELECTRIC MIXTURES CONTAINING CONDUCTING PARTICLES AT OPTICAL FREQUENCIES (POSTPRINT)

M.Y. Koledintseva, R.E. DuBroff, and R.W. Schwartz

JUNE 2006

MATERIALS AND MANUFACTURING DIRECTORATE
AIR FORCE RESEARCH LABORATORY
AIR FORCE MATERIEL COMMAND
WRIGHT-PATTERSON AIR FORCE BASE, OH 45433-7750

REPORT DOCUMENTATION PAGE

Form Approved
OMB No. 0704-0188

1. REPORT DATE *(DD-MM-YY)*	2. REPORT TYPE	3. DATES COVERED *(From - To)*
June 2006	Journal Article Postprint	

4. TITLE AND SUBTITLE
MAXWELL GARNETT MODEL FOR DIELECTRIC MIXTURES CONTAINING CONDUCTING PARTICLES AT OPTICAL FREQUENCIES (POSTPRINT)

5a. CONTRACT NUMBER
FA8650-04-C-5704

5b. GRANT NUMBER

5c. PROGRAM ELEMENT NUMBER
78011F

6. AUTHOR(S)
M.Y. Koledintseva, R.E. DuBroff, and R.W. Schwartz

5d. PROJECT NUMBER
2865

5e. TASK NUMBER
25

5f. WORK UNIT NUMBER
25100000

7. PERFORMING ORGANIZATION NAME(S) AND ADDRESS(ES)
University of Missouri-Rolla
B. 37 McNutt Hall
1870 Miner Circle
Rolla, MO 65409-0340

8. PERFORMING ORGANIZATION REPORT NUMBER

9. SPONSORING/MONITORING AGENCY NAME(S) AND ADDRESS(ES)
Materials and Manufacturing Directorate
Air Force Research Laboratory
Air Force Materiel Command
Wright-Patterson AFB, OH 45433-7750

10. SPONSORING/MONITORING AGENCY ACRONYM(S)
AFRL-ML-WP

11. SPONSORING/MONITORING AGENCY REPORT NUMBER(S)
AFRL-ML-WP-TP-2006-445

12. DISTRIBUTION/AVAILABILITY STATEMENT
Approved for public release; distribution is unlimited.

13. SUPPLEMENTARY NOTES
This paper was submitted to the Journal of Laser Applications.
PAO Case Number: AFRL/WS 06-1319, 16 May 2006.

14. ABSTRACT
Mathematical modeling of composites made of a dielectric base and randomly oriented metal inclusions is considered. Different sources of frequency dependency of metal conductivity at optical frequencies are taken into account. These include the skin-effect, dimensional (length-size) resonance of metal particles, and the Drude model. Also, mean free path of electrons in metals can be smaller than the characteristic sizes of nanoparticles, and this leads to the decrease in conductivity of metal inclusions. These effects are incorporated in the Maxwell Garnett mixing formulation, and give degrees of freedom for forming desirable optical frequency characteristics of composite media containing conducting particles.

15. SUBJECT TERMS
mathematical modeling, dielectric base, skin effect dimensional

16. SECURITY CLASSIFICATION OF:			17. LIMITATION OF ABSTRACT:	18. NUMBER OF PAGES	19a. NAME OF RESPONSIBLE PERSON (Monitor)
a. REPORT	b. ABSTRACT	c. THIS PAGE			Mary E. Kinsella
Unclassified	Unclassified	Unclassified	SAR	34	19b. TELEPHONE NUMBER *(Include Area Code)* N/A

Standard Form 298 (Rev. 8-98)
Prescribed by ANSI Std. Z39-18

Maxwell Garnett Model for Dielectric Mixtures Containing Conducting Particles at Optical Frequencies

Marina Y. Koledintseva, Richard E. DuBroff, and Robert W. Schwartz

University of Missouri-Rolla, USA

Abstract

Mathematical modeling of composites made of a dielectric base and randomly oriented metal inclusions is considered. Different sources of frequency dependency of metal conductivity at optical frequencies are taken into account. These include the skin-effect, dimensional (length-size) resonance of metal particles, and the Drude model. Also, mean free path of electrons in metals can be smaller than the characteristic sizes of nanoparticles, and this leads to the decrease in conductivity of metal inclusions. These effects are incorporated in the Maxwell Garnett mixing formulation, and give degrees of freedom for forming desirable optical frequency characteristics of composite media containing conducting particles.

I. INTRODUCTION

Engineering composite materials with desirable electromagnetic properties for different applications from radio frequencies to the optical range has become one of the most important problems of modern science and technology.

There are many different effective medium theories used for modeling electromagnetic properties of composites. One of them is the Maxwell Garnett model [1], which is simple and convenient for modeling due to its linearity. The Maxwell Garnett model is valid for dielectric composites with dilute conductive phases (below the percolation threshold). This is a model that implies the quasistatic approximation. Its main features are

- the mixture is electrodynamically isotropic;
- the mixture is linear, that is, none of its constitutive parameters depends on the intensity of electromagnetic field;
- the mixture is non-parametric, that is, its parameters do not change in time according to some law as a result of external forces – electrical, mechanical, etc.;
- inclusions are separated by distances greater than their characteristic size;
- the characteristic size of inclusions is small compared to the wavelength in the effective medium;
- inclusions are arbitrary randomly oriented ellipsoids;
- if there are conducting inclusions, their concentration should be lower than the percolation threshold.

Maxwell Garnett formalism has been successfully applied to engineering microwave absorbing materials containing carbon particles [2],

$$\varepsilon_{ef} = \varepsilon_b + \frac{\frac{1}{3}\sum_{i=1}^{n} f_i(\varepsilon_i - \varepsilon_b)\sum_{k=1}^{3}\frac{\varepsilon_b}{\varepsilon_b + N_{ik}(\varepsilon_i - \varepsilon_b)}}{1 - \frac{1}{3}\sum_{i=1}^{n} f_i(\varepsilon_i - \varepsilon_b)\sum_{k=1}^{3}\frac{N_{ik}}{\varepsilon_b + N_{ik}(\varepsilon_i - \varepsilon_b)}}, \qquad (1)$$

where ε_b is the relative permittivity of a base dielectric; ε_i is the relative permittivity of the i-th sort of inclusions; f_i is the volume fraction occupied by the inclusions of the i-th type; N_{ik} are the depolarization factors of the i-th type of inclusions, and the index k=1,2,3 corresponds to x,y, and z Cartesian coordinates. Equation (1) is generalized for a multiphase mixture schematically shown in Figure 1. The constitutive parameters of the base material and inclusions can be functions of frequency.

Formulas for calculating depolarization factors of ellipsoids and the table of depolarization factors for canonical spheroids (spheres, disks, and cylinders) can be found in [3]. Equation *(1)* allows that within the same composite material, particles can have different depolarization factors. However, in reality it is almost impossible to have perfect ellipsoidal or spheroidal particles, so, for any arbitrary shape a reasonable approximation is needed. If the inclusions are thin rods (cylinders), their two depolarization factors are close to $N_{i1,2} \approx 1/2$, and the third depolarization factor can be calculated as in [4], $N_{i3} \approx (1/a)^2 \ln(a)$. Herein, $a = l/d$ is the aspect ratio of an inclusion, l is its length, and d is the diameter.

The dielectric properties of the conducting inclusions are described by the complex relative permittivity

$$\varepsilon_i(j\omega) = \varepsilon_i' - j\varepsilon_i'' = \varepsilon_i' - j\frac{\sigma_i}{\omega\varepsilon_0}, \qquad (2)$$

the real part of which is much smaller than the imaginary part ($\varepsilon_i' << \sigma_i/(\omega\varepsilon_0)$). In (2), σ_i is the bulk conductivity of inclusions.

It has been shown that by varying conductivity, aspect ratio, and concentration of inclusions it is possible to form the desirable frequency characteristics of composites, including shielding effectiveness. Application of the genetic algorithms allows for optimization of the mixture contents to achieve the highest possible shielding effectiveness [5].

Mixtures of randomly oriented nanosize conducting particles at concentrations far below the percolation threshold can still be treated using Maxwell Garnett formalism at optical frequencies, but some corrections in the model must be introduced. Thus, the model should take into account peculiarities of the conductive particles behavior at optical frequencies, which may differ considerably from their behavior at microwave

frequencies. Also, dimensional resonance in the particles of inclusions might greatly influence the effective permittivity of the composite.

The structure of the paper is the following. Section II contains the mathematical model of the composite taking the abovementioned effects into account. The results of calculations based on this model are presented and discussed in Section III. The conclusions are summarized in Section IV.

II. MATHEMATICAL MODEL

2.1. Renormalized conductivity taking the skin effect into account

At the microwave frequencies, the skin effect in the conducting inclusions can be neglected. However, at the optical frequencies currents induced by the electromagnetic waves in the conducting particles exist only in very thin surface layers, while the bulk of the particle is not involved in interaction. For this reason, the skin effect is substantial and influences the frequency dependence of the particle.

Skin depth is calculated as

$$\delta(\omega) = \sqrt{\frac{2}{\omega\mu_i\mu_0\sigma_i}}. \qquad (3)$$

Lagarkov and Sarychev [6], according to [7, Section 61], introduced the renormalized conductivity to take the skin effect into account (see Figure 2). Renormalized conductivity is related to the bulk conductivity as

$$\begin{aligned} \sigma_{skin} &= \sigma_i \cdot f(\Delta); \\ \Delta &= d/(2\delta(\omega)); \\ f(\Delta) &= \frac{1-j}{\Delta} \cdot \frac{J_1((1+j)\Delta)}{J_0((1+j)\Delta)}, \end{aligned} \qquad (4)$$

where $J_{0,1}$ are the Bessel functions of the zero and the first order, respectively. This renormalized conductivity appears to be a complex value, and it is dependent on frequency through $\delta(\omega)$. This is the basic difference between the microwave and optical behavior of metals: the conductivity of metals at optical frequencies is not constant, it depends on frequency.

$$\sigma_{skin}(\omega) = \sigma'_{skin}(\omega) + j\sigma''_{skin}(\omega). \qquad (5)$$

The real part of conductivity is responsible for ε'', while the imaginary part contributes to ε'.

2.2. Conductivity taking into account small size of nanorods compared to mean free path of electrons

Since the inclusions of interest are nanorods, they are so thin that their diameter could be smaller than the electron mean free path. Then, instead of the bulk conductivity, the corrected conductivity should be taken into account,

$$\sigma_{free} = \Lambda \sigma_i, \tag{6}$$

where the coefficient Λ is a function of the ratio

$$\Lambda = f\left(b_i / L_{free}\right), \tag{7}$$

where b_i is the inclusion characteristic size ($d \le b_i \le l$) along the vector of the electric field acting on the mixture, and $L_{free} = v_F \tau_0$ is the mean free path for electrons in the conductor [8].

For randomly oriented conducting particles, it can be assumed that the one-third of all particles have their characteristic dimension in the direction of the incident electric field close to $b_i \approx d$, which leads to the decrease of conductivity up to two times. One-third of all particles have $b_i > L_{free}$, so that their conductivity is close to the bulk conductivity. And the remainder have an average characteristic dimension of $b_i = \frac{l+d}{2}$, which can lead to some decrease of conductivity. Thus, the coefficient Λ may be even smaller than is given in the tables in [8], if surface roughness and grain size of metal inclusion are taken into account [9-11]. For our computations, we assume that reasonable value is $\Lambda = 0.8$, that is, corresponding to a 20% decrease in conductivity. Figure 3 taken from [11, Fig. 1] shows that when the technology node decreases in size and becomes comparable to the mean free path of electrons in metals (for majority of metals, such as Cu, Ag, Pt, Au, Al, etc. it is in the range of 10-100 nm at room temperature), the resistivity of metal components substantially increases, since surface, grain boundary, and barrier layer effects become substantial.

In such cases, it is reasonable to replace the bulk conductivity σ_i in (3) and (4) by σ_{free}, since the actual conductivity of the nanosize metal inclusion might be lower than the bulk conductivity. Consequently,

$$\sigma_{skin} = \sigma_{free} \cdot f(\Delta); \text{ and } \delta(\omega) = \sqrt{\frac{2}{\omega \mu_i \mu_0 \sigma_{free}}}. \tag{8}$$

2.3. Drude model for metals at optical frequencies

It is known that the frequency dependence of metals over the optical frequency range is described by the Drude model [12-15].

$$\varepsilon_i(j\omega) = 1 - \frac{\omega_p^2}{\omega(\omega - j\gamma)}, \tag{9}$$

where ω_p is the angular plasma frequency for free electrons, and γ is the angular relaxation frequency. The relaxation frequency is $\gamma = 1/\tau$, where τ is the resonance relaxation time. From (9), real and imaginary parts of complex permittivity are

$$\begin{aligned} &\varepsilon_i(j\omega) = \varepsilon_i' - j\varepsilon_i'';\\ &\varepsilon_i' = 1 - \frac{\omega_p^2}{\omega^2 + \gamma^2};\\ &\varepsilon_i'' = \frac{\omega_p^2 \gamma}{\omega\left(\omega^2 + \gamma^2\right)} \end{aligned} \tag{10}$$

The imaginary part in (10) can be represented as usual

$$\varepsilon_i'' = \frac{\sigma_D}{\omega\varepsilon_0}, \tag{11}$$

where Drude conductivity is

$$\sigma_D = \frac{\varepsilon_0 \omega_p^2 \gamma}{\left(\omega^2 + \gamma^2\right)}. \tag{12}$$

The total conductivity of a metal particle is comprised of "low-frequency" conductivity and Drude conductivity that is substantial at the higher optical frequencies. These two conductivities contribute to the total permittivity independently, because their effects are separated in frequency.

$$\varepsilon_i(j\omega) = \varepsilon_i' - j\varepsilon_i'';$$
$$\varepsilon_i' = \varepsilon_D' + \varepsilon_{skin}' = 1 - \frac{\omega_p^2}{\omega^2 + \gamma^2} + \frac{\sigma_{skin}''}{\omega\varepsilon_0};$$
$$\varepsilon_i'' = \varepsilon_D'' + \varepsilon_{skin}'' = \frac{\omega_p^2\gamma}{\omega\left(\omega^2 + \gamma^2\right)} + \frac{\sigma_{skin}'}{\omega\varepsilon_0} = \frac{\sigma_\Sigma}{\omega\varepsilon_0}; \qquad (13)$$
$$\sigma_\Sigma = \sigma_D + \sigma_{skin}'.$$

Data for the plasma frequency and Drude relaxation frequency for metals can be taken from the graphs and tables in papers [14, 15]. In these papers, the Drude model parameters ω_p and γ are given in [cm^{-1}] units, so that $\omega[1/cm] = \dfrac{\omega[rad/s]\cdot 10^{-2}}{2\pi\cdot c[m/s]}$.

2.4. Dimensional resonance in metal particles

Electromagnetic resonance in the particles of inclusions is another source of frequency dependence of composites. An inclusion particle in the form of a nanorod can be represented as an electric dipole antenna. Suppose that nanorods are non-interacting, corresponding to a sparse concentration of inclusions in the base material. Let us calculate equivalent conductivity of an inclusion particle. This conductivity then can be used in Maxwell Garnett formulation for the effective permittivity.

According to [16,17], any inclusion particle can be described by its antenna dipole input impedance. This is a series connection of radiation resistance R_W, capacitance of the wire C_i and its inductance L_i.

$$Z_{in} = R_{rad} + j\omega L_i + \frac{1}{j\omega C_i}. \qquad (14)$$

For a dipole antenna these values are approximately calculated as in [18],

$$R_{rad} = 20\pi^2\sqrt{\varepsilon_{ef}}\left(\frac{l}{\lambda_0}\right)^2, \text{[Ohms]}; \; C_i = \frac{\pi\varepsilon_0\varepsilon_{ef}l}{2\ln(2a)}, \text{[F]}; \quad L_i = \frac{\mu_0 l}{6\pi}\left(\ln(2a) - \frac{11}{6}\right), \text{[H]}. \qquad (15)$$

It is known that if the inclusions are small compared with wavelength, their input impedance is mainly capacitive. Radiation resistance determines effectiveness of the dipole radiation, and it will contribute to the real part of the permittivity of the composite.

The rigorous formulation for radiation resistance and reactance of a dipole antenna of any length can be found in [19, Section 21.2], and these parameters can be calculated using numerical integration. Thus, the input impedance can be calculated as

$$Z_{in} = \frac{j\eta}{4\pi \sin^2 kh} \int_{-h}^{h} F(z)dz, \tag{16}$$

where the integrand is

$$F(z) = \left[\frac{e^{-jkR_1}}{R_1} + \frac{e^{-jkR_2}}{R_2} - 2\cos kh \frac{e^{-jkR_0}}{R_0} \right] \sin(k(h - |z|)). \tag{17}$$

The distances are calculated as

$$\begin{aligned} R_0 &= \sqrt{(d/2)^2 + z^2}; \\ R_1 &= \sqrt{(d/2)^2 + (z-h)^2}; \\ R_2 &= \sqrt{(d/2)^2 + (z+h)^2}. \end{aligned} \tag{18}$$

In (16)-(18), $\eta = 120\pi \sqrt{\frac{\varepsilon_{ef}}{\mu_{ef}}}$ (for dielectric composite $\mu_{ef} = 1$), $h = l/2$ is an antenna half-length, and $k = \frac{2\pi}{\lambda_{ef}} = \frac{2\pi}{\lambda_0}\sqrt{\varepsilon_{ef}}$ is the wave number in the effective medium. It should be mentioned that ε_{ef} in (15)-(17) are taken from calculating effective permittivity using the Maxwell Garnett formula (1) before the dipole antenna effect is taken into account.

In [16], the polarizability of dipole particles is introduced as

$$\alpha_{ee} = \frac{l_{ef}^2}{j\omega Z_{in}} \text{ [F} \cdot \text{m}^2\text{]}, \tag{19}$$

where l_{ef} is the effective dipole antenna length. For small dipoles, it can be assumed that $l_{ef} \approx l/2$. For dipoles with $l = \lambda/2$, $l_{ef} = 0.637(2l) = 1.274l$ [20, Section 9.2] For longer dipole antennas, the effective length is $l_{ef} = 2.558l^2/\lambda$. (An effective length of a dipole antenna is calculated through the antenna with the homogeneous current distribution along the dipole, and the same area under the current distribution function along the dipole length).

The conductivity of particles due to the dimensional resonance can be calculated by equating the effective permittivity of a sparse conglomerate of the identical conductive particles (neglecting the base material) with polarizability α_{ee} and a concentration of n particles per unit volume,

$$\varepsilon = \varepsilon_0 \left(1 + \frac{n}{\varepsilon_0} \alpha_{ee} \right) = \varepsilon_0 \left(\varepsilon' - j \frac{\sigma_{res}}{\omega \varepsilon_0} \right), \tag{20}$$

For cylindrical particles,

$$n = f_i / v_i = \frac{4 f_i}{\pi d^2 l}, \text{ [1/m}^3\text{]}. \tag{21}$$

Then, the conductivity associated with the dimensional resonance is

$$\sigma_{res} = j\omega n \alpha_{ee} \text{ , [S/m]}. \tag{22}$$

Substituting (15) and (19) in (22), one can get conductivity associated with the dimensional resonance as

$$\sigma_{res} = \frac{n l_{ef}^2}{Z_{in}} = \frac{4 f_i l_{ef}^2}{\pi d^2 l Z_{in}}. \tag{23}$$

This is a complex value $\sigma_{res} = \sigma'_{res} + j\sigma''_{res}$, and it can be added to the formula (13), describing the total conductivity σ_Σ. Its real part contributes to the loss in the material, and the imaginary contributes to the real part of the composite permittivity, associated with phase velocity of electromagnetic waves propagation. This means that when α_{ee} is real (no loss), Z_{in} is imaginary (purely reactive), then σ_{res} is real and contributes to loss in the material. When α_{ee} is imaginary (only loss), Z_{in} is real (pure radiation resistance), and then σ_{res} is imaginary and contributes to the real part of permittivity of the composite.

2.5. Frequency characteristic of the base material

The frequency characteristics of the base material also have an impact on the frequency characteristics of the mixture. Depending on the base material used for making the composite, and the frequency range of its application, this base material can be modeled as a lossless nondispersive medium, as a lossy Debye material, as a resonance Lorentzian medium, or as their superposition.

The Debye frequency characteristic for a dielectric base material is

$$\varepsilon_b = \varepsilon_{\infty b} + \frac{\varepsilon_{sb} - \varepsilon_{\infty b}}{1 + j\omega\tau_D}, \tag{24}$$

where ε_{sb} and $\varepsilon_{\infty b}$ are static and high-frequency ("optic") relative permittivities of the material, and τ_D is the Debye relaxation time. In the case of a Lorentzian material, it is described as

$$\varepsilon_b = \varepsilon_{\infty b} + \frac{(\varepsilon_{sb} - \varepsilon_{\infty b})\omega_{0b}^2}{\omega_{0b}^2 - \omega^2 + 2j\omega\delta_b}, \qquad (25)$$

where ω_{0_b} is the angular resonance frequency of the base material, and $(2\delta_b)$ is the resonance line width at -3 dB level.

If the base material resonance is pronounced and comparatively narrow in the frequency range of interest (narrowband Lorentzian material, for which $\omega_0 = \omega_p > (2\delta)$ [22]), it might have a great impact on the frequency-selective properties of the composite. If the dielectric is wideband Lorentzian ($\omega_0 = \omega_p < (2\delta)$), then its behavior is very close to the Debye frequency dependence [22].

III. RESULTS OF COMPUTATIONS

A program in Matlab has been developed to calculate reflection and transmission coefficients from a slab of a composite material containing metal particles (nanorods). Below there are the modeled results that take into account all the abovementioned effects.

Figure 6 shows the reflection and transmission coefficients for a layer of the modeled composite material 1 μm thick. The input data for computations are the following: the bulk conductivity of silver particles is $\sigma_i = 6.3 \cdot 10^7$ S/m; the coefficient Λ taking the mean free path into account is assumed to be Λ=0.8; the mean free path of electrons of silver is taken as 40 nm; the aspect ratio of the inclusions is $a = 50$; the length of the particles $l = 1$ μm; and the diameter of the particles is assumed to be $d = 20$ nm. The volume fraction of the inclusions is $f_i = 0.7/a$, which is below the percolation threshold estimated as $p_c = 4.5/a$ [6]. The parameters for polymethylmethacrylate (PMMA) base material taken for these computations are the Debye parameters: $\varepsilon_S = 2.2$, $\varepsilon_\infty = 1.9$, and $\tau_{Debye} = 10^{-14}$ s. It should be mentioned that PMMA is known to be almost transparent in the visual frequency band (98% transparency), while in UV range it almost non-transparent (wideband Lorentzian behavior with $\omega_0 \approx 2 \cdot 10^{16}$ Hz). The dispersive curves for PMMA at optical and UV frequencies can be found in [21].

Frequency dependence of reflectance, transmittance, and absorbance (magnitude, resonance frequency, and width of the resonance line) greatly depend on the Drude parameters for silver - ω_p and γ_{Drude}. Skin effect plays an important part for comparatively low-frequency absorption and frequency selectivity. Resonance of inclusions falls into the frequency range of interest and contributes to the absorption and radiation by inclusion dipole antennas. This contribution is affected by the geometry of inclusions.

Figure 7 shows the influence of the material of inclusions on the absorbance, defined as $A = \log_{10}(P_t / P_{inc})$ in bels. The Drude parameters for different metals - silver, copper, gold, aluminum, and platinum – are found in [15] and presented here in Table 1. The base material was PMMA, and the inclusion particles had an aspect ratio of a=50, a length of l=1 μm, and a diameter of d=20 nm. The volumetric fraction of the inclusions

was $f_i = 0.7/a$. The composites containing metal particles with higher bulk conductivity will absorb energy more effectively.

Figure 8 shows that the frequency dependence of the shielding effectiveness can be also controlled by varying the size of the inclusions. It is important that the higher aspect ratio of inclusions does not necessarily yield greater shielding effectiveness, as happens in the microwave range [2]. At optical frequencies, the longer particles of inclusions radiate more effectively than the shorter ones, and this radiation contributes to the real part of the effective permittivity of the composite, rather than its imaginary part responsible for absorption in the material.

Table 1

Conductivity and Drude Model Parameters for Some Metals

Metal	Bulk conductivity, $10^{-6}\cdot\sigma$ S/m	$10^{-16}\cdot\omega_p$, 1/m	$10^{-12}\cdot\gamma$, 1/m
Ag	63.05	1.369	27
Cu	57.0	1.122	13
Au	45.55	1.37	40
Al	36.5	2.24	120
Pt	9.59	0.78	105

Figure 9 demonstrates the effect of the length of inclusions on the absorbance. The diameter of inclusions for all the curves is 20 nm. The dimensional resonance in the particles corresponds to the peak of absorption. Thus, for particles having length l=1000 nm, the resonance frequency corresponds to a wavelength of about 375 nm. When particles are shorter, this peak shifts to the shorter wavelengths. The absorbance decreases in the frequency range of interest for shorter inclusions, since the number of Ag particles per unit volume (concentration) is kept constant ($4.45\cdot10^{19}\,m^{-3}$). Thus, the volumetric fraction of conducting inclusions decreases when they are shorter.

Figures 10 and 11 show the influence of Ag particles on the frequency characteristic of a mixture, when the model for PMMA base material is nondispersive (Figure 10) and is described by the Debye dispersion law (Figure 11). The base material itself is almost transparent in the frequency range of interest.

Figure 12 contains the absorbance characteristics for a Lorentzian-type base material, for a conglomerate comprised solely of Ag particles of the same size and volumetric fraction as in Figures 10 and 11, and the mixture of the base and the Ag inclusions. The frequency dependence for a composite is a superposition of the frequency characteristics of its phases. In reality, PMMA behaves more like a Lorentzian material in the UV range, where it becomes nontransparent. In the visual band, it is still appropriate to describe it as non-dispersive or slightly-dispersive with the Debye-like frequency dependence.

Figure 13 contains absorbance characteristics for composites with different Debye characteristics of the base material. In the graphs shown in the figure, the static permittivity is a varying parameter. It is seen that increase of ε_{sb} leads not only to the higher absorption in a wider band, but also to the shift of the peak of absorption to the shorter wavelengths. However, it can be seen that substantial increase in ε_{sb} (from 2.2 to 8.2) does not significantly change the absorption characteristic.

Figure 14 shows the frequency dependence of absorbance, when different models of base materials are taken into account. There is almost no difference in the curves for PMMA model taken as the Debye (curve 1) and the wideband Lorentzian frequency dependence (curve 3). The size of the Ag particles was the same as in Figure 7 (aspect ratio a=50, the length l=1 μm, and the diameter d=20 nm). The narrow absorption peak (curves 3 and 6) can be obtained using narrowband Lorentzian base material. This can be achieved at $\omega_{0b} = \omega_{pb} > (2\delta)$. If it is possible to find a dielectric with a Lorentzian peak at visible frequencies, then it would enhance the absorption by the silver particles. This problem might be solved, for example, by adding Ag particles in colored optical glass base [23].

IV. CONCLUSION

Frequency-dependent parameters of composites containing 3D randomly oriented conducting inclusions (nanorods) at optical frequencies can be modeled using Maxwell Garnett formulation, if the concentration of inclusions is smaller than the percolation threshold. The frequency-dependent permittivity of a mixture mainly depends on the conductivity of the metal inclusions. Behavior of metal inclusions at optical frequencies greatly differs from that at microwaves. Nanosize metal inclusions exhibit frequency dependence because of the skin-effect and free electron plasma resonance phenomena described by the Drude model. Also, an inclusion particle behaves as a resonant scatterer, so its dipole antenna model should be taken into account. In addition, the mean free path of electrons in metals may be smaller than the characteristic size of metal inclusions, and this will substantially decrease the conductivity of the metals. All these effects are incorporated in the Maxwell Garnett mixing formulation, and give degrees of freedom for forming frequency characteristics of composite media containing conducting particles.

References

1. J.C.Maxwell Garnett, "Colours in metal glasses and metal films", Philos. Trans. R. Soc. London, Sect. A, vol. 3, pp.385-420, 1904.
2. M.Y.Koledintseva, P.C.Ravva, R.E.DuBroff, J.L.Drewniak, K.N.Rozanov, and B.Archambeault, "Engineering of composite media for shields at microwave frequencies", *Proc. IEEE EMC Symposium*, August 2005, Chicago, IL, vol. 1, pp. 169-174.
3. M.Y.Koledintseva, J.Wu, J.Zhang, J.L.Drewniak, and K.N.Rozanov, "Representation of permittivity for multi-phase dielectric mixtures in FDTD

modeling", Proc. IEEE Symp. Electromag. Compat., 9-13 Aug. 2004, Santa Clara, CA, vol. 1, pp.309-314, 2004.

4. S.M.Matitsine, K.M.Hock, L.Liu, et.al., "Shift of resonance frequency of long conducting fibers embedded in a composite", J. Appl. Phys., vol. 94, no.2, pp. 1146-1154, 2003.
5. J.Huang, M.Y.Koledintseva, P.C.Ravva, J.L.Drewniak, R.E.DuBroff, B.Archambeault, and K.N.Rozanov, "Design of a metafilm-composite dielectric shielding structure using a genetic algorithm", *Progress in Electromagnetic Research Symposium (PIERS)*, Cambridge, MA, USA, 26-29 March 2006, Full papers (accepted).
6. A.N.Lagarkov and A.K.Sarychev, "Electromagnetic properties of composites containing elongated conducting inclusions", *Phys. Review B*, vol. 53, no. 9, March 1996, pp. 6318-6336.
7. L.D.Landau, E.M.Lifshitz, and L.P.Pitaevskii, *Electrodynamics of Continuous Media*, 2nd ed., Oxford, New York: Pergamon, 1984.
8. D.Gottlieb and V.Halpern, "The electrical conductivity of very thin metal films", *J. Phys. F: Metal. Phys.*, vol. 6, no. 12, 1976, pp. 2333-2339.
9. Chen and D. Gardner, "Influence of line dimensions on the resistance of Cu interconnections", *IEEE Electr. Dev. Lett.*, vol. 19, no. 12, 1998, p.508.
10. Kapur, J. P. McVittie and K. C. Saraswat, "Technology and reliability constrained future copper interconnects—Part I: Resistance modeling", *IEEE Trans. Electr. Dev.*, vol. 49, no. 4, 2002, pp. 590-597.
11. S.Im, N.Srivastava, K.Banerjee, and K.Goodson, "Thermal Scaling Analysis of Multilevel C/Low-k Interconnect Structures in Deep Nanometer Scale Technologies", *Proc. 22th Int. VLSI Multilevel Interconnect Conf. (VMIC),* Oct. 3-6, Fremont, CA, pp. 525-530, 2005.
12. R.Zhang, S. Dods, and P.Catrysse, "FDTD approach for optical metallic material", *Laser Focus World*, July 2004, p.68 (www.laserfocusworld.com).
13. G.Veronis, R.W.Dutton, and S. Fan, "Metallic photonic crystals with strong broadband absorption at optical frequencies over wide angular range", *J. Appl. Phys.*, vol. 97, no. 9, 2005.
14. M.A.Ordal, L.L.Long, R.J.Bell, S.E. Bell, R.R.Bell, R.W.Alexander, Jr., and C.A.Ward, "Optical properties of the metals Al,Co,Au,Fe,Pb,Ni,Pd,Pt,Ag,Ti, and W in the infrared and far infrared", *Appl.Optics*, vol. 22, no. 7, April 1983, pp. 4493-4499.
15. M.A.Ordal, R.J.Bell, R.W.Alexander, Jr., L.L.Long, and M.R.Querry, "Optical properties of the metals Al,Co,Au,Fe,Pb,Ni,Pd,Pt,Ag,Ti, and W in the infrared and far infrared", *Appl.Optics*, vol. 24, no. 24, Dec.1985, pp. 1099-1120.
16. S.A.Tretyakov, F.Mariotte, C.R.Simovski, T.G.Kharina, and J.-P. Heliot, "Analytical antenna model for chiral scatterers: comparison with numerical and experimental data", *IEEE Trans. Antennas and Propagat.*, vol. 44, no. 7, July 1996, pp. 1006-1014.
17. S.A.Tretyakov, "Metamaterials with wideband negative permittivity and permeability", *Microw. Opt. Techn. Lett.*, vol. 31, no. 3, Nov. 2001, pp. 163-165.
18. R.W.P.King and C.W.Harrison, *Antennas and Waves: A Modern Approach.* Cambridge, MA: MIT Press, 1969.

19. S.J.Orfanidis, *Electromagnetic Waves and Antennas*, published on website www.ece.rutgers.edu/~orfanidi/ewa
20. D.M.Sazonov, *Anntennas and Microwave Devices*, Moscow, Russia: Vysschaya Shkola, 1988 (in Russian).
21. J.J.Risko, L.J.Brillson, R.W.Bigelow, and T.J.Fabish, "Electron energy loss spectroscopy and the optical properties of polymethylmethacrylate from 1 to 300 eV", J. Chem Phys., vol. 69, no. 9, Nov. 1978, pp. 3931-3939.
22. M.Y.Koledintseva, J.L.Drewniak, D.J.Pommerenke, K.N. Rozanov, G.Antonini, and A.Orlandi, "Wideband Lorentzian Media in the FDTD Algorithm", *IEEE Trans. Electromag. Compat.*, vol. 47, no. 2, May 2005, pp. 392-398.
23. *Colored Optical Glass*, http://www.lzos.ru/en/glass_color.htm

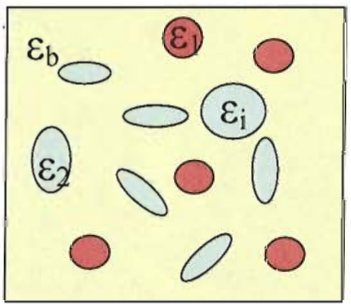

Figure 1. Schematic of a multiphase mixture

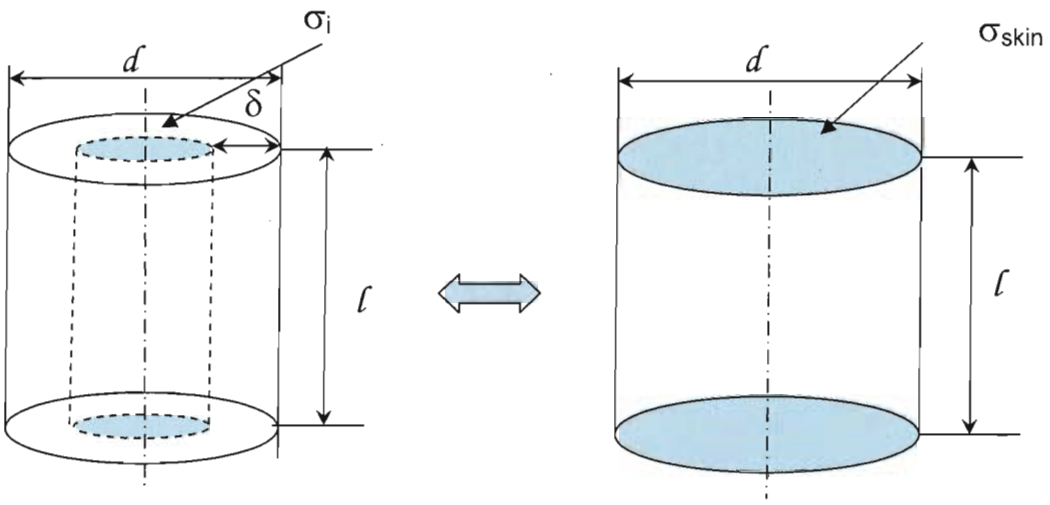

Figure 2. Renormalization of conductivity due to the skin-effect.

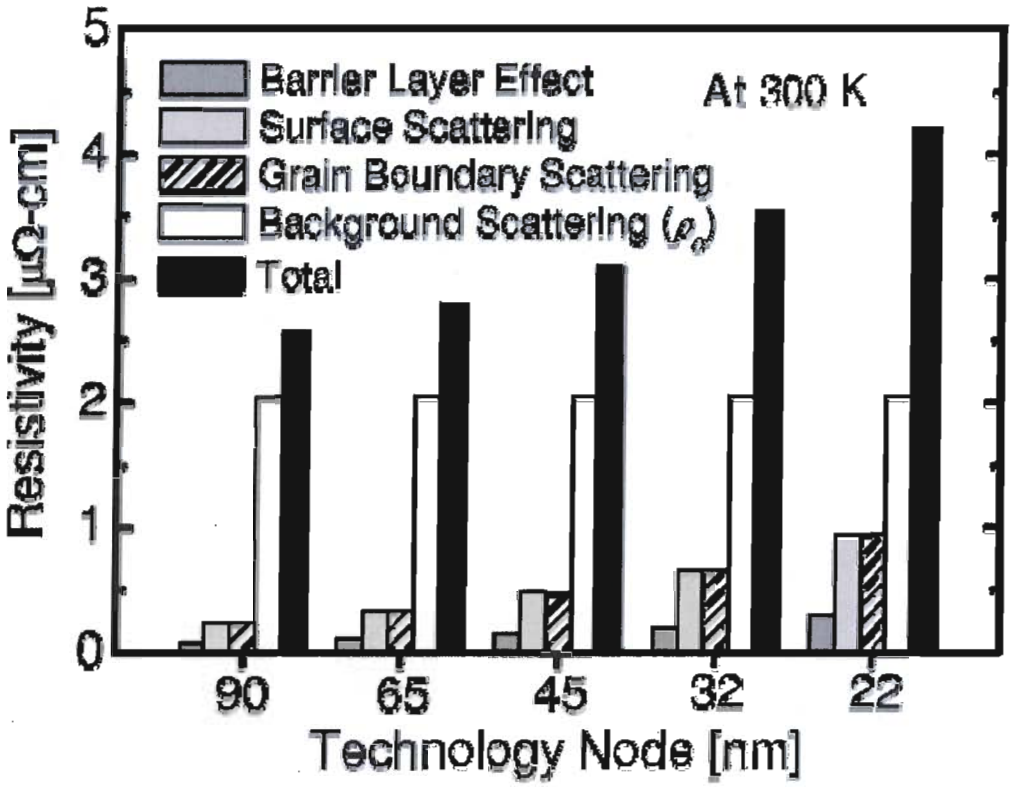

Figure 3. Increase of resistivity of metals (herein - copper) for elements of small size [11].

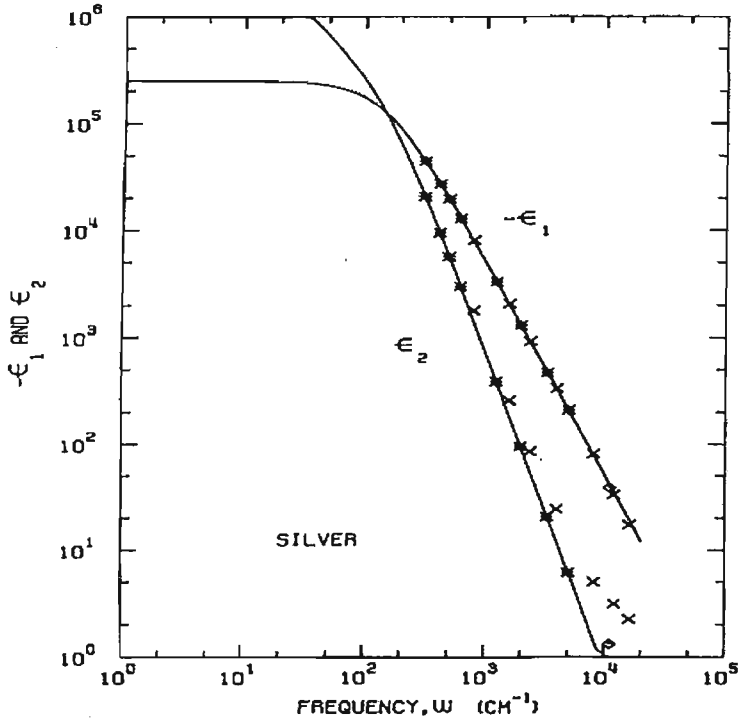

Silver: $-\epsilon_1(\omega)$ and $\epsilon_2(\omega)$ vs frequency. The solid line is the Drude model. The data from Ref. 11 are: Bennett and Bennett, ✱ for both $-\epsilon_1$ and ϵ_2; Schulz, ◇ for both; and Hagemann *et al.*, × for both.

Figure 4. Real and imaginary parts of permittivity for Drude model of silver [14, Fig 5]. References are made on the paper cited in [14].

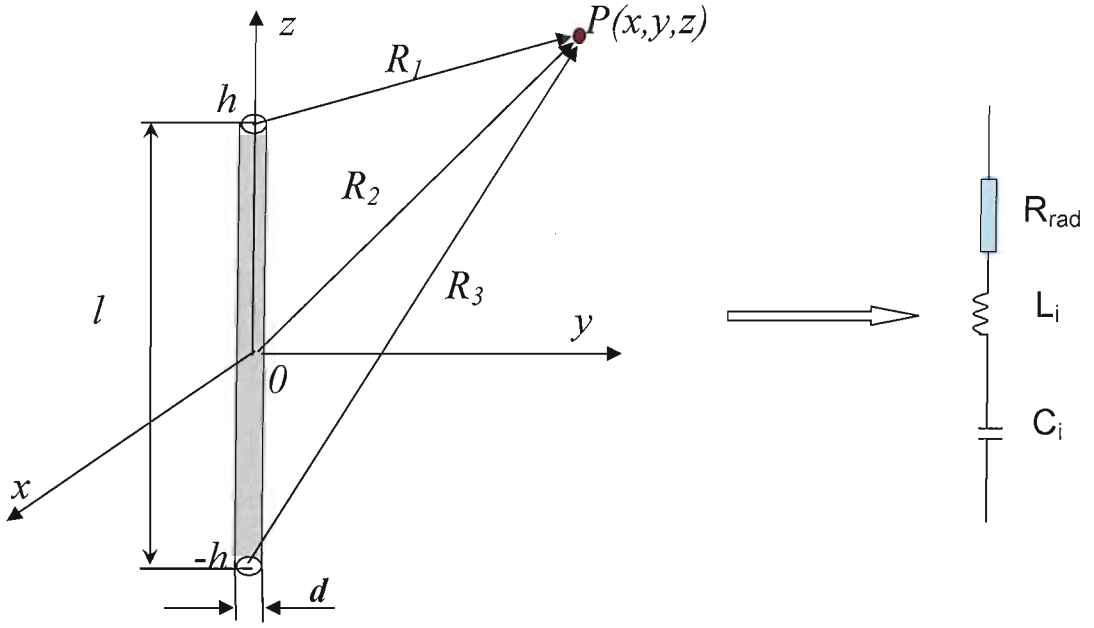

Figure 5. Analogy of an inclusion particle and a dipole antenna

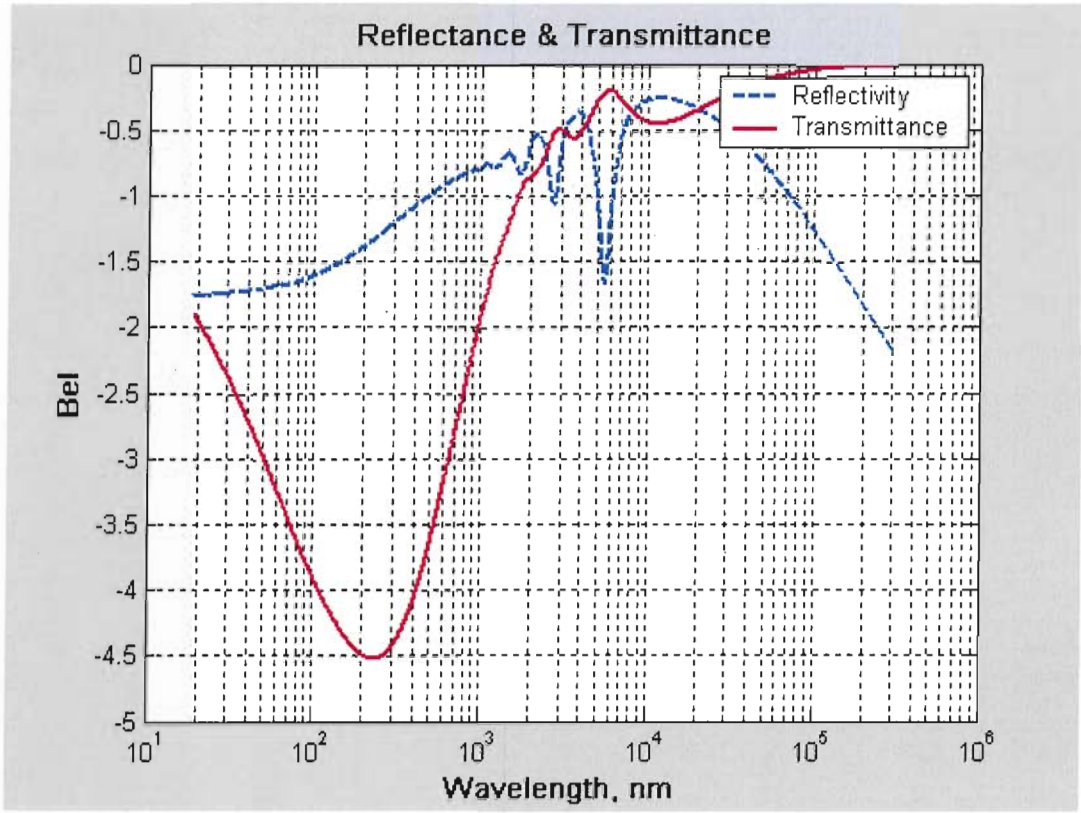

Figure 6. Reflectance and transmittance characteristics for a 1-μm-thick slab of a composite material PMMA-Ag.

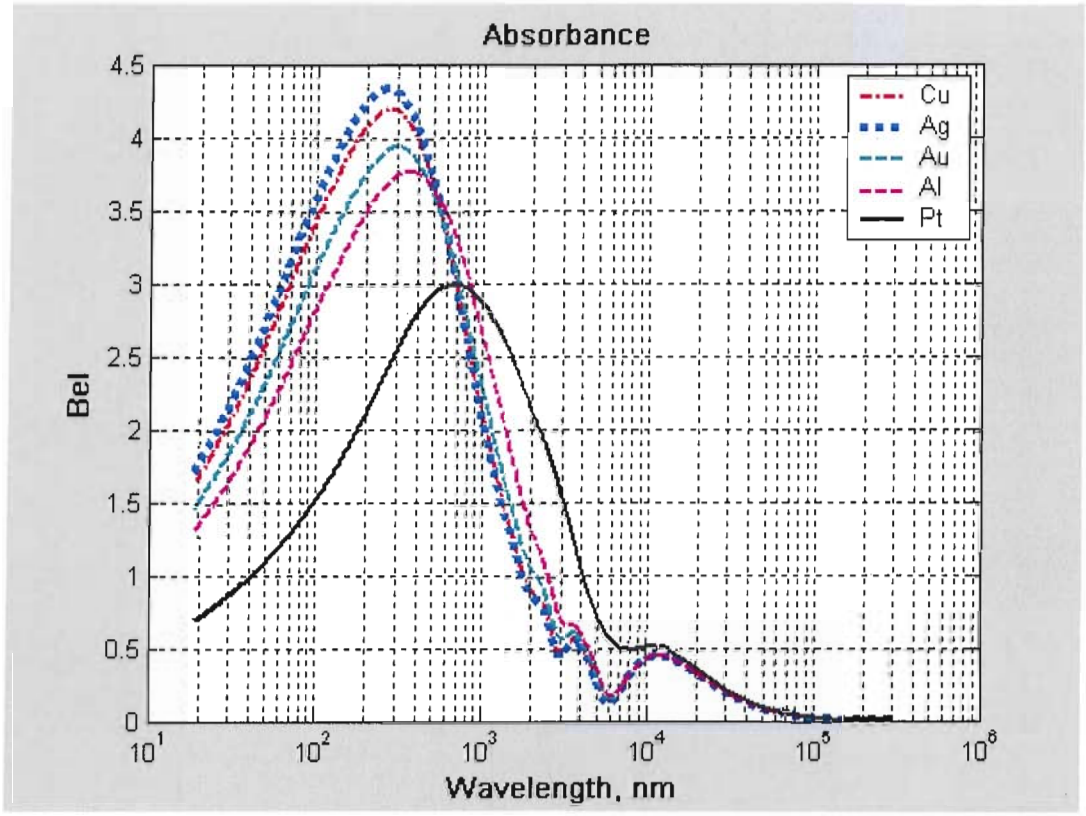

Figure 7. Absorbance for a 1 μ m- thick slab of a composite material - PMMA base and different metals as inclusions.

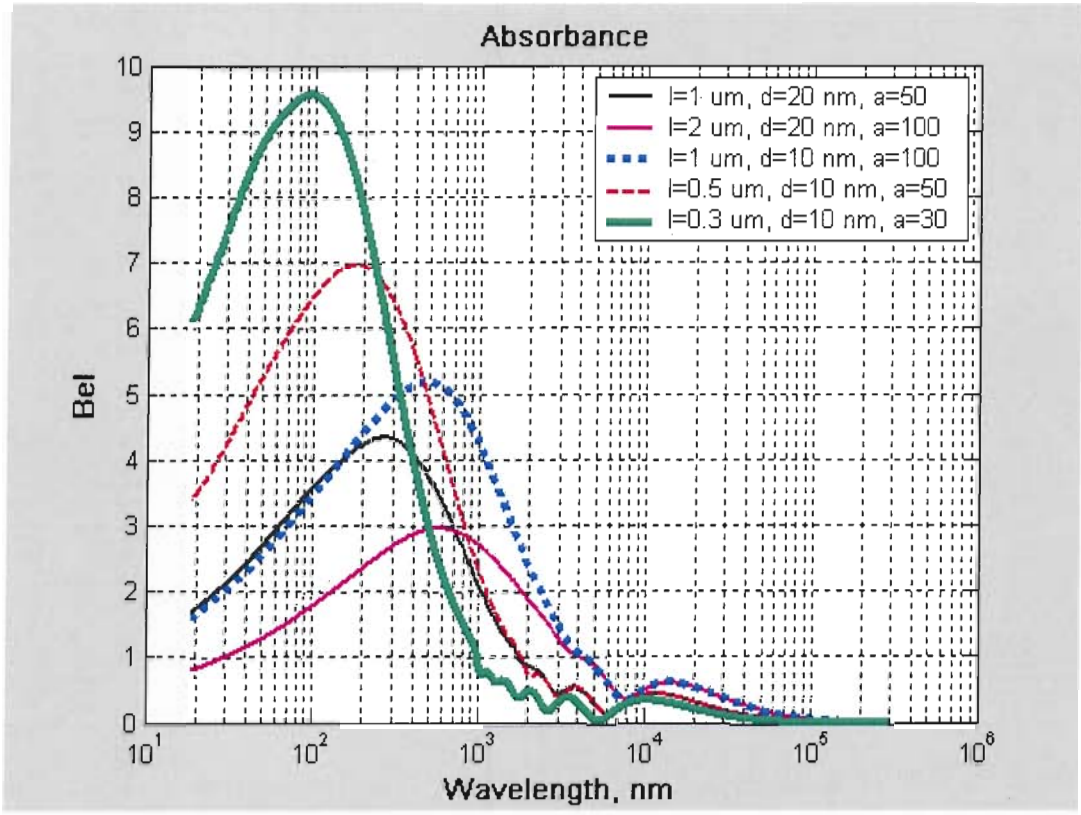

Figure 8. Absorbance control by varying the size of inclusions. Volumetric fraction is $f_i = 0.7/a$. The layer thickness is 1 μm.

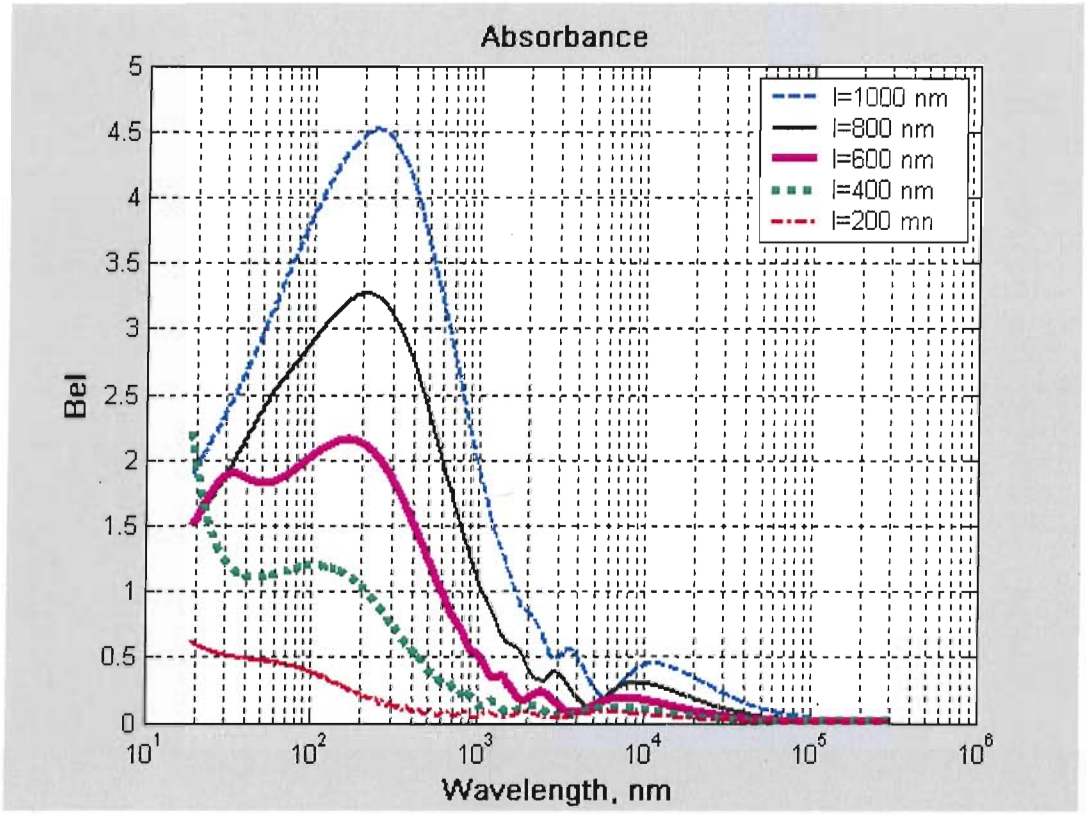

Figure 9. Absorbance as a function of wavelength for a 1 μ m-thick composite layer PMMA-Ag; parameter l is the length of Ag inclusions; the concentration of Ag particles is const $=4.45 \cdot 10^{19}\ \mathrm{m}^{-3}$.

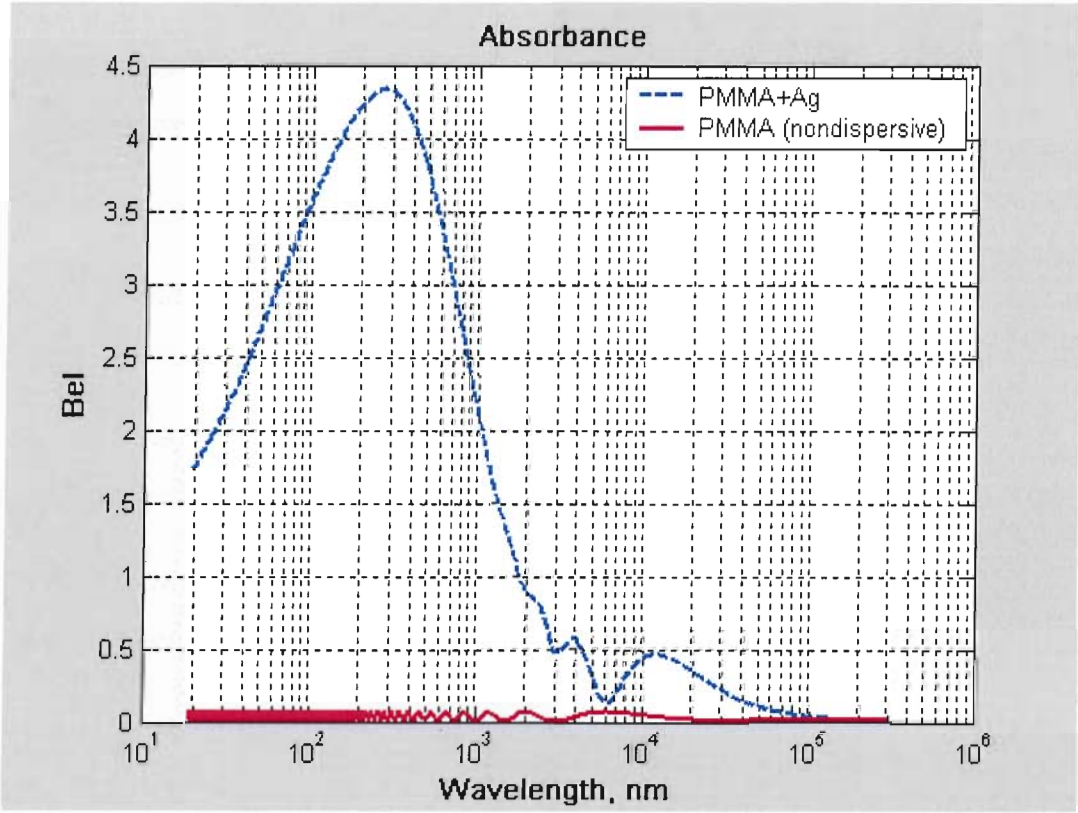

Figure 10. PMMA – nondispersive ($\varepsilon_{sb} = 2.2$); Ag particles ($a = 50$; $l = 1\,\mu$m; $d = 20$ nm); concentration $n_i = 4.45 \cdot 10^{-19}\,\mathrm{m}^{-3}$; ($f_i = 0.7/a$) for a 1-μm thick slab.

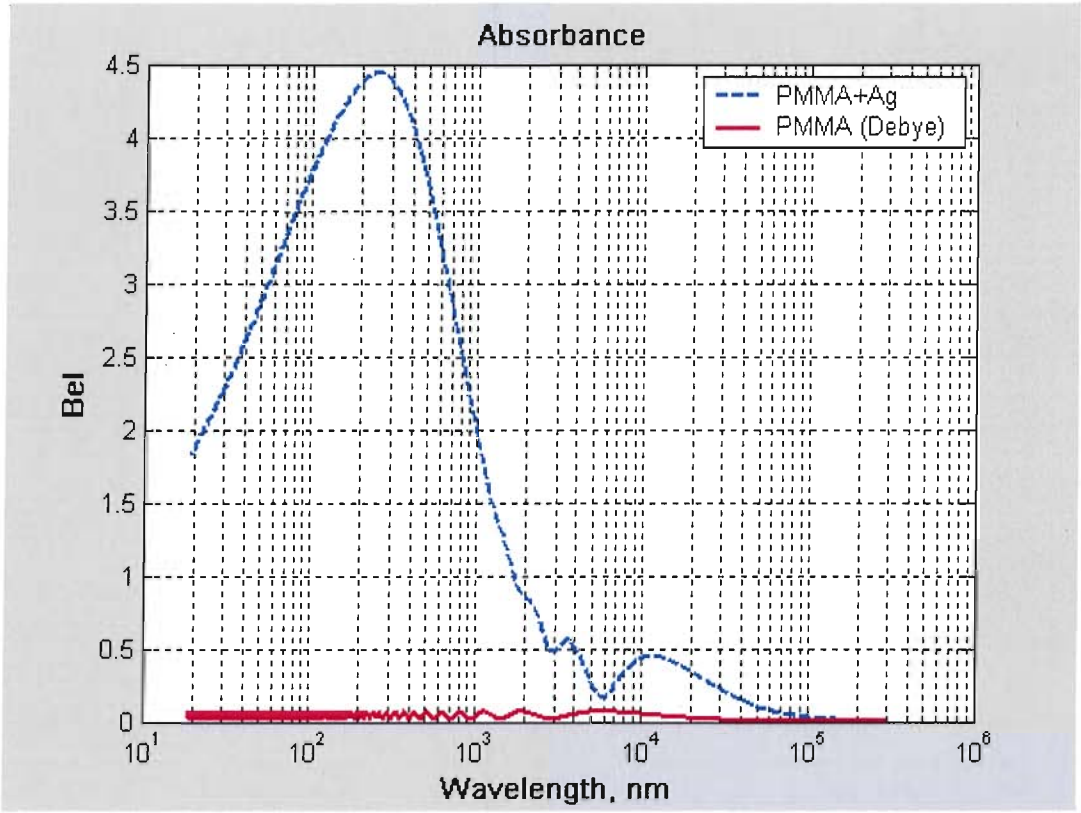

Figure 11. PMMA – Debye ($\varepsilon_{sb} = 2.2, \varepsilon_{\infty b} = 1.9$, $\tau = 1 \cdot 10^{-14}$ 1/s); Ag particles ($a = 50$; $l = 1\,\mu$m; $d = 20$ nm); concentration $n_i = 4.45 \cdot 10^{-19}\,\mathrm{m}^{-3}$ ($f_i = 0.7/a$) for a 1-μm thick slab.

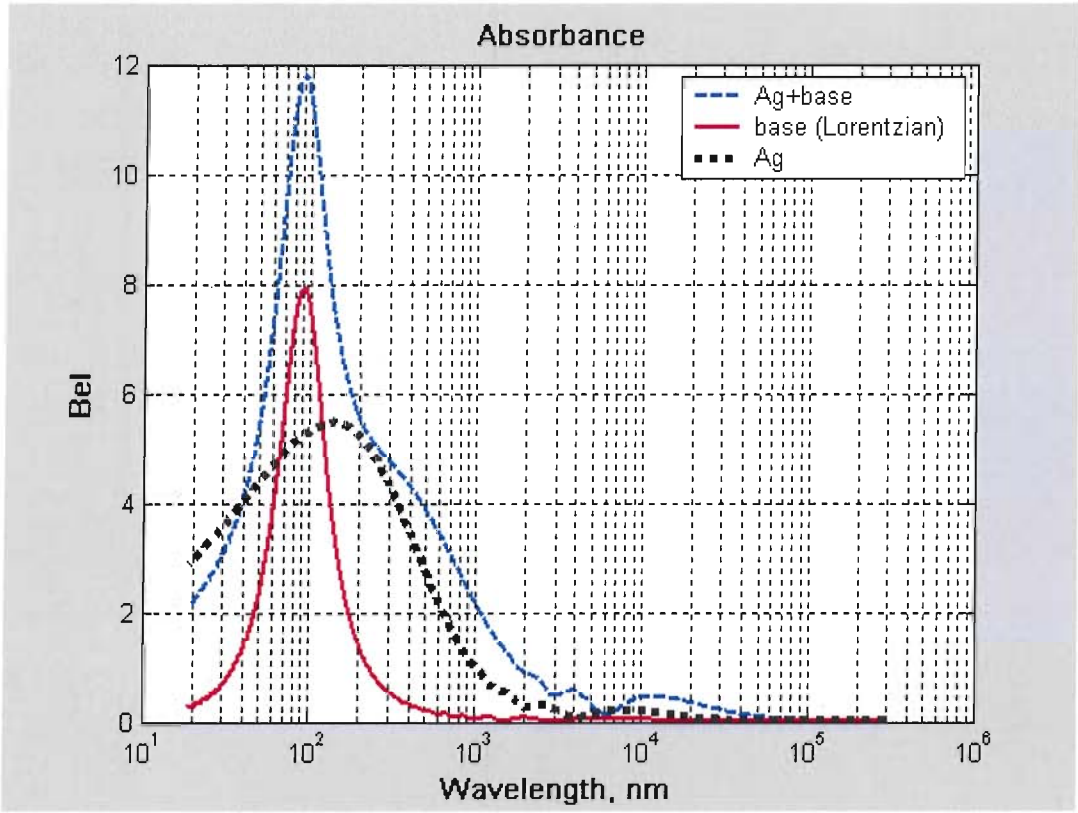

Figure 12. Dielectric – Lorentzian ($\varepsilon_{sb} = 2.2$, $\varepsilon_{\infty b} = 1.9$, $\omega_{0b} = \omega_{pb} = 2.05 \cdot 10^{16}$ rad/s; $\delta_b = 1.67 \cdot 10^{16}$ rad/s;) Ag particles ($a = 50$; $l = 1\,\mu$m; $d = 20$ nm); concentration $n_i = 4.45 \cdot 10^{-19}\,\mathrm{m}^{-3}$ ($f_i = 0.7/a$) for a 1-μm thick slab.

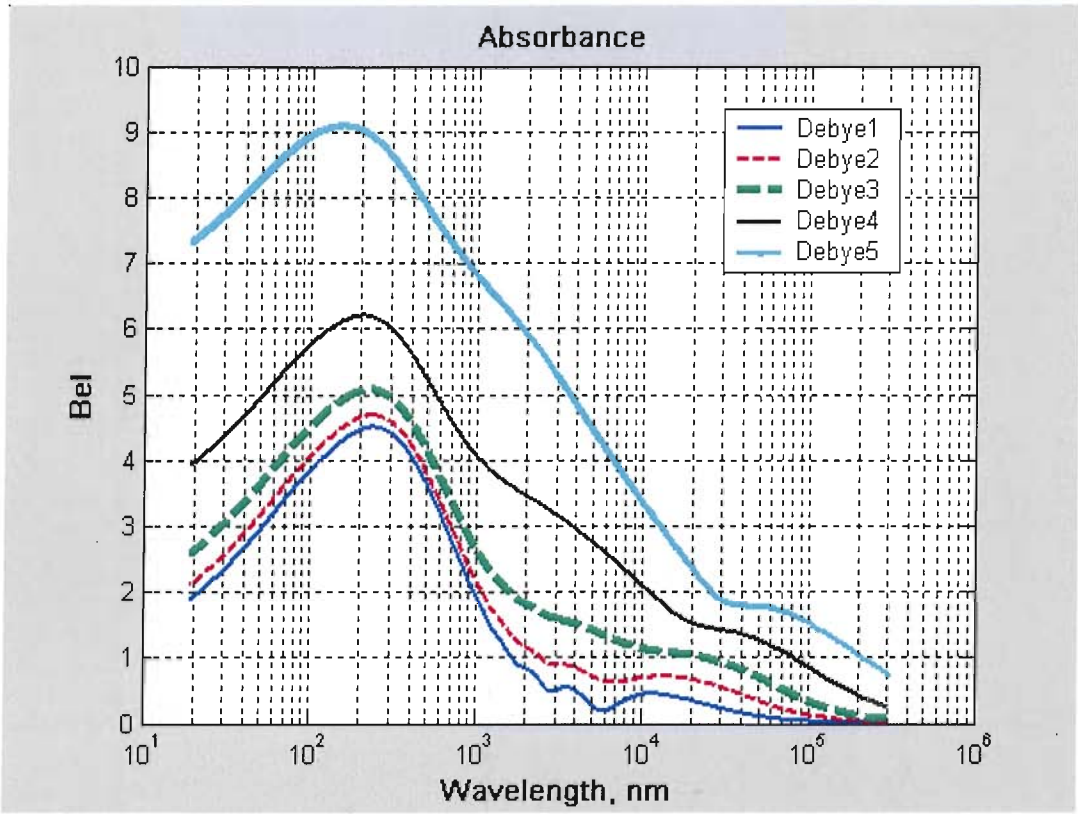

Figure 13. Ag particles ($a = 50$; $l = 1\,\mu$m; $d = 20$ nm); concentration $n_i = 4.45 \cdot 10^{-19}$ 1/m^3 ($f_i = 0.7/a$) for a 1-μm thick slab for five different base materials, denoted as Debye1 through Debye 5 corresponding to $\varepsilon_{sb} = 2.2$, 4.2, 8.2, 20.2, and 50.2. The parameters $\varepsilon_{\infty b} = 1.9$ and $\tau = 1 \cdot 10^{-14}$ 1/s are the same for all the five cases.

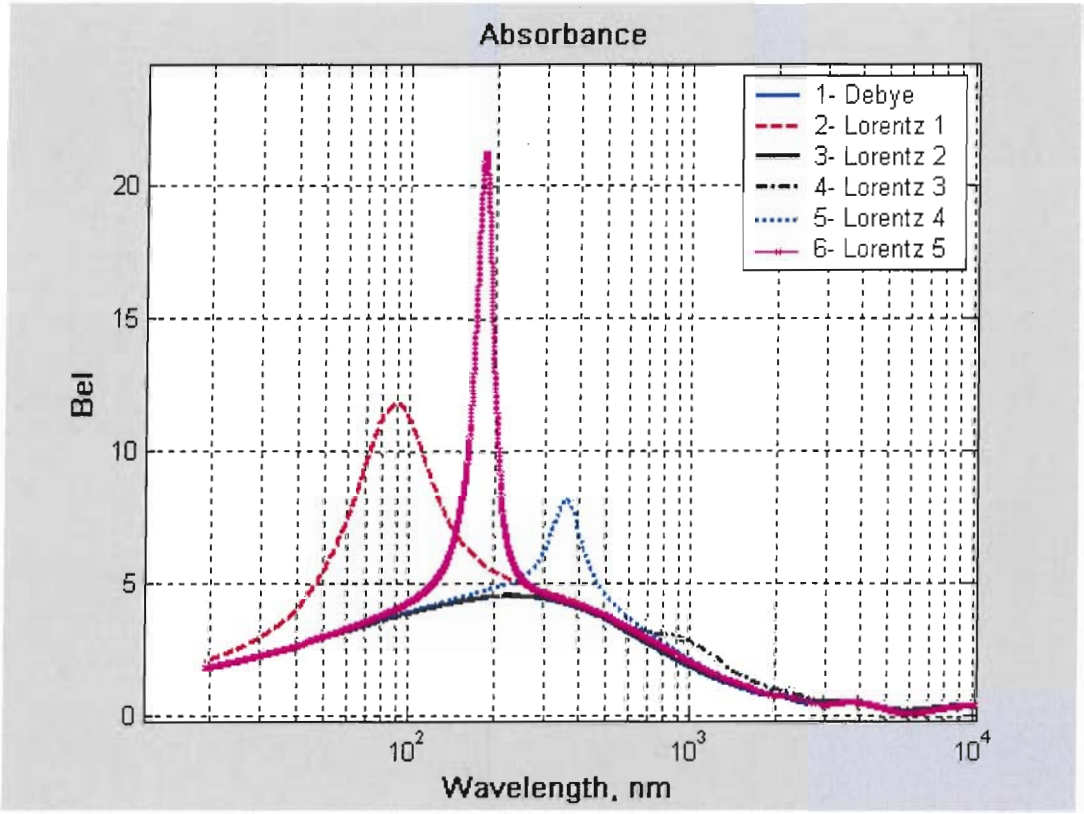

Figure 14. Ag particles ($a = 50$; $l = 1\,\mu$m; $d = 20$ nm); concentration $n_i = 4.45 \cdot 10^{-19}$ m^{-3} ($f_i = 0.7/a$) for a 1-μm thick slab with five different base materials: **1**- PMMA - Debye; **2**- Lorentzian 1: $\varepsilon_{sb} = 2.2$, $\varepsilon_{\infty b} = 1.9$, $\omega_{0b} = \omega_{pb} = 2.05 \cdot 10^{16}$ rad/s; $\delta = 1.67 \cdot 10^{16}$ rad/s; **3** –Lorentzian 2: $\varepsilon_{sb} = 2.2$, $\varepsilon_{\infty b} = 1.9$, $\omega_{0b} = \omega_{pb} = 2.05 \cdot 10^{15}$ rad/s; $\delta_b = 1.67 \cdot 10^{16}$ rad/s; **4** - Lorentzian 3: $\varepsilon_{sb} = 2.2$, $\varepsilon_{\infty b} = 1.9$, $\omega_{0b} = \omega_{pb} = 2.05 \cdot 10^{15}$ rad/s; $\delta_b = 1.67 \cdot 10^{15}$ rad/s; **5** –Lorentzian 4: $\varepsilon_{sb} = 2.2$, $\varepsilon_{\infty b} = 1.9$, $\omega_{0b} = \omega_{pb} = 5.0 \cdot 10^{15}$ rad/s; $\delta_b = 1.67 \cdot 10^{15}$ rad/s; **6** – Lorentzian 5: $\varepsilon_{sb} = 2.2$, $\varepsilon_{\infty b} = 1.9$, $\omega_{0b} = \omega_{pb} = 10.0 \cdot 10^{15}$ rad/s; $\delta_b = 1.67 \cdot 10^{15}$ rad/s.